Journal of Sound and Vibration (1998) **215**(3), 455–473
Article No. sv981643

DYNAMIC CHARACTERISTICS AND MODE LOCALIZATION OF ELASTICALLY CONSTRAINED AXIALLY MOVING STRINGS AND BEAMS

C. H. Riedel and C. A. Tan

Department of Mechanical Engineering, Wayne State University, Detroit, MI 48202, *U.S.A.*

(*Received* 17 *November* 1997, *and in final form* 12 *March* 1998)

The free vibration response of an axially moving string and Euler–Bernoulli beam supported by an intermediate elastic constraint is studied. The transfer function method is used to formulate the free response solution. For the beam, the elastic constraint can consist of either a transverse spring or both transverse and rotational springs. The effects of both speed and tension on mode localization are studied. A wave analysis is employed to further investigate the behaviour of the systems. Reflection and transmission coefficients are formulated to show the effects of the system parameters on the coupling of the subsystems. The addition of the constraint is shown to increase the critical speed of the beam for low values of tension. For the string, mode localization increases as speed increases. However, the behaviour of the beam is shown to change significantly depending on both the system parameters and type of constraint. The effects of tension and speed on the delocalization frequency of the weakly bi-coupled beam are also presented.

1. INTRODUCTION

Many mechanical systems which are used to transmit power, information or materials do so with the use of a flexible translating element. These elements are commonly referred to as *axially moving materials*. The translating string and translating Euler–Bernoulli beam are the two most common models of axially moving materials used to describe the dynamics of such systems as belts, chains, fibres, magnetic tapes, and band saws. These basic models belong to the class of gyroscopic systems which experience a divergence instability at a critical speed where the fundamental natural frequency vanishes. The vibration and stability of axially moving materials have often focused on a single span translating with constant velocity between two fixed supports [1, 2]. A comprehensive review on the dynamics of axially moving materials is found in reference [3].

However, in many applications such as conveyor belts, the element translates over multiple supports. The supports may be rigid or elastic. In these cases, there are multiple spans coupled by intermediate supports and the resulting motion may be quite complex. As a result, multi-span axially moving systems have also been treated to address the issues of coupling and stability. Translating strings coupled by point springs and elastic foundations have shown that these constraints do not alter the critical speed of the system [4, 5]. However, the critical speed changes when the translating string is coupled by a pulley with a complaint support [6]. Translating beams and plates have been used to study band/wheel systems. Early studies neglected the coupling between spans and focused on just a single span [2, 7]. However, it was shown that finite curvature of the spans, due to the bending of the band around the wheels, is essential for coupling of the transverse

0022–460X/98/330455 + 19 $30.00/0

vibrations to occur and that the coupling is significant [8, 9]. Also, when the wheels are mounted on compliant supports and allowed to translate, the band tension in general depends on both velocity and the stiffness of the wheel support. This results in a critical speed which depends on the stiffness of the wheel support. Other factors which affect the coupling are band geometry and material properties, transport speed, axial band tension, and support stiffness [10, 11].

The coupling phenomena have also been studied in the context of mode localization. In terms of coupling, the spans of the string are mono-coupled through transverse displacement, while the beam may be mono- or bi-coupled through transverse displacement and/or rotation. Mode localization of mono-weakly-coupled, nearly periodic systems has received much attention [12–19]. The existence of mode localization and the degree of localization have been shown to depend on both the amount of disorder and the coupling strength [19]. Only recently, however, have the issues of mode localization and eigenvalue veering in axially moving materials been addressed. Cheng and Perkins [20] applied a perturbation technique to the characteristic equation to examine the eigenvalue veering and flutter instability for a friction guided, translating string coupled by a point spring. Tan and Zhang [21] employed a similar approach to study the eigenvalue veering of a point-constrained string translating across an elastic foundation and the coupling dynamics between the subsystems. Mode localization of a translating string coupled to stationary constraints is studied in reference [22]. Al-Jawi *et al*. [23] studied both a cyclic and non-cyclic two-span axially moving beam coupled by an intermediate simple support. Their system was mono-coupled in rotation and the disorder was due to the tension difference between the spans. Differences between the cyclic and non-cyclic cases were discussed and the effects of speed and tension on the localization were examined. While most research has focused on the mode localization in mono-coupled systems, the dynamic characteristics of a stationary, bi-coupled beam were studied in reference [24]. To date, the mode localization of a multi-span, bi-coupled, axially moving beam has not been reported in the literature.

The above studies indicate that depending on the modelling and type of supports, the coupling behaviour and stability of multi-span axially moving materials can be significantly different. While the effects of various intermediate support conditions for axially moving strings have been studied extensively, the vibrations of elastically constrained axially moving beams have received less attention. Recently, it is shown that different support conditions result in significant changes in the behaviour of a beam [24]. In particular, a mode delocalization phenomenon occurs for certain support conditions. The purpose of this paper is to extend reference [24] to the problem of a two-span axially moving material. The subsystems are coupled by elastic point springs. For the beam, the effects of both transverse and rotational constraints on the critical speed and mode localization are examined. The effects of system parameters, in particular speed and tension, on the coupling of the subsystems are also studied. Due to the extensive amount of existing research on the string model, the majority of this paper is dedicated to the beam model. While new results pertaining to the string model are presented, it is possible that some of the results could have been gleaned from previous work. The primary reason in presenting these results is to examine and compare the similarities that exist between the string and the beam under certain conditions.

This paper is organized as follows. In section 2 the problem formulation and governing equations of motion are presented. Employing the transfer function method [25, 26], the free response solution of the system is derived in section 3. The effects of the coupling elements on the critical speed are presented in section 4. Fundamental characteristics of mode localization are studied in section 5. A wave propagation analysis is used to

determine the reflection and transmission coefficients at the subsystem interface. This analysis provides insight on how various system parameters affect the behaviour of the system at both low and high frequencies. Section 6 shows the effects of the system parameters on the mode delocalization.

2. PROBLEM FORMULATION

A schematic of the system to be studied is shown in Figure 1. This system represents a string or an Euler–Bernoulli beam translating with a constant speed V between two fixed end supports a distance L apart and under a constant, uniform tension P_o. The string or beam is constrained by pointwise linear transverse and/or rotational springs (for beams) at X_c. The transverse and rotational spring constants are denoted by K_t and K_r, respectively. Assumptions for both models include: (1) the mass per unit length ρ is constant; (2) the equilibrium position is straight; (3) damping is neglected. All speeds considered are below the critical speed.

The transfer function method [26] is used to formulate the problem and give the free response of the constrained axially moving material. With this formulation, the system is partitioned into two subsystems, as illustrated in Figure 1. Under the above assumptions, the non-dimensional equation of motion governing the transverse displacement $w(x, t)$ of each subsystem is

$$\left(\frac{\partial^2}{\partial t^2} + G\frac{\partial}{\partial t} + K\right)w(x, t) = f_e(x, t), \qquad x\in(0, x_c), \quad x\in(x_c, 1), \tag{1}$$

with boundary conditions expressed in the general form

$$M_j w(x, t)|_{x=0} + N_j w(x, t)|_{x=1} = \gamma_{Bj}(t), \qquad t \geqslant 0, \quad j = 1, \ldots, n, \tag{2}$$

where n is the highest order of derivatives in x. M_j and N_j are spatial, linear differential operators of the proper order and $\gamma_{Bj}(x, t)$ are functions describing the inhomogeneous boundary conditions. For fixed supports, $\gamma_{Bj}(x, t) = 0$. In equation (1), $f_e(x, t)$ is the transverse force, K and G are the stiffness and gyroscopic spatial differential operators, respectively:

string model: $$K = (c^2 - 1)\frac{\partial^2}{\partial x^2}, \qquad G = 2c\frac{\partial}{\partial x}; \tag{3a}$$

beam model: $$K = (c^2 - p_o)\frac{\partial^2}{\partial x^2} + \frac{\partial^4}{\partial x^4}, \qquad G = 2c\frac{\partial}{\partial x}. \tag{3b}$$

The non-dimensional parameters for the string are

$$w = W/L, \qquad x = X/L, \qquad t = T\sqrt{P_o/\rho L^2}, \qquad c = V\sqrt{\rho/P_o}, \qquad k_t = K_t L/P_o \tag{4a}$$

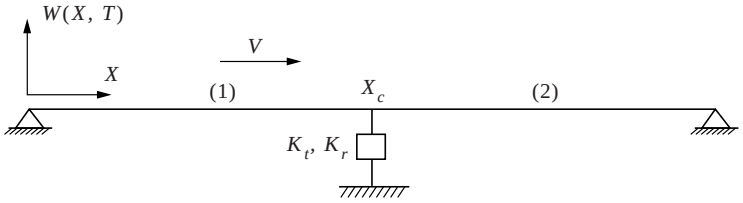

Figure 1. A translating string or beam constrained by an intermediate elastic support.

and for the beam,

$$w = W/L, \qquad x = X/L, \qquad t = T\sqrt{EI/\rho L^4}, \qquad c = V\sqrt{\rho L^2/EI}, \qquad p_o = P_o L^2/EI,$$
$$k_t = K_t L^3/EI, \qquad k_r = K_r L/EI. \tag{4b}$$

Based on the transfer function method, the generalized displacement and force for the string are $w(x, t)$ and $w_{,x}(x, t)$, respectively. For the beam, the generalized displacements are $w(x, t)$ and $w_{,x}(x, t)$ while the generalized forces are $w_{,xx}(x, t)$ and $w_{,xxx}(x, t)$. The constraint conditions at x_c are the continuity of generalized displacements and the balance of generalized forces which are determined as follows.

string model:
$$(1 - c^2)(w_{,x}(x_c^+, t) - w_{,x}(x_c^-, t)) = k_t w(x_c, t); \tag{5}$$

beam model:
$$w_{,xx}(x_c^-, t) - w_{,xx}(x_c^+, t) = -k_r w_{,x}(x_c, t), \tag{6a}$$
$$w_{,xxx}(x_c^-, t) - w_{,xxx}(x_c^+, t) = k_t w(x_c, t). \tag{6b}$$

3. FREE RESPONSE ANALYSIS

According to the transfer function method, first transform the global co-ordinate x into a local co-ordinate $z \in (0, 1)$ for each subsystem, and represent the Laplace transformed equations (1) and (2) in the state space form. Define $\boldsymbol{\eta}^{(i)}(z, s)$ as the state vector where, for the string,

$$\boldsymbol{\eta}^{(i)}(z, s) = \{\bar{w}^{(i)}(z, s)\ \bar{w}^{(i)}_{,z}(z, s)\}^T, \tag{7}$$

and for the beam,

$$\boldsymbol{\eta}^{(i)}(z, s) = \{\bar{w}^{(i)}(z, s)\ \bar{w}^{(i)}_{,z}(z, s)\ \bar{w}^{(i)}_{,zz}(z, s)\ \bar{w}^{(i)}_{,zz}(z, s)\}^T; \tag{8}$$

$\bar{w}^{(i)}(z, s)$ is the Laplace transform form of $w(z, t)$ for the ith subsystem. The response solution for each subsystem is [25]

$$\boldsymbol{\eta}^{(i)}(z, s) = \int_0^1 G^{(i)}(z, \xi, s)\mathbf{q}^{(i)}(\xi, s)\, \mathrm{d}\xi + H^{(i)}(z, s)\boldsymbol{\gamma}^{(i)}(s), \qquad z \in (0, 1), \tag{9}$$

where the matrix transfer functions $G^{(i)}(z, \xi, s)$ and $H^{(i)}(z, s)$ are given by

$$G^{(i)}(z, \xi, s) = \begin{cases} H^{(i)}(z, s)M^{(i)}(s)\, \mathrm{e}^{-F^{(i)}(s)\xi}, & \xi < z, \\ -H^{(i)}(z, s)N^{(i)}(s)\, \mathrm{e}^{F^{(i)}(s)1-\xi}, & \xi > z, \end{cases} \tag{10a}$$

$$H^{(i)}(z, s) = \mathrm{e}^{F^{(i)}(s)z}(M^{(i)}(s) + N^{(i)}(s)\, \mathrm{e}^{F^{(i)}(s)})^{-1}. \tag{10b}$$

The state matrices $F^{(i)}(s)$ and boundary operators $M^{(i)}(s)$, $N^{(i)}(s)$ are listed in the Appendix. In equation (9), $\mathbf{q}^{(i)}(\xi, s)$ and $\boldsymbol{\gamma}^{(i)}(s)$ are the state vectors for excitations and inhomogeneous boundary conditions, respectively.

Equations (9) and (10a, b) give the formal, closed-form solution of the response for each subsystem. For free vibration analysis, $\mathbf{q}^{(i)}(\xi, s) = 0$ and the boundary conditions at $x = 0$ and 1 are homogeneous. The response of each subsystem is obtained from equation (9):

$$\boldsymbol{\eta}^{(i)}(z, s) = H^{(i)}(z, s)\boldsymbol{\gamma}^{(i)}(s), \qquad z \in (0, 1), \tag{11}$$

where for the string model:

$$\boldsymbol{\gamma}^{(1)}(s) = \begin{Bmatrix} 0 \\ \bar{w}(x_c, s) \end{Bmatrix}, \qquad \boldsymbol{\gamma}^{(2)}(s) = \begin{Bmatrix} \bar{w}(x_c, s) \\ 0 \end{Bmatrix}, \tag{12a}$$

and the beam model:

$$\boldsymbol{\gamma}^{(1)}(s) = \begin{Bmatrix} 0 \\ 0 \\ \bar{w}(x_c, s) \\ \bar{w}_{,x}(x_c, s) \end{Bmatrix}, \qquad \boldsymbol{\gamma}^{(2)}(s) = \begin{Bmatrix} \bar{w}(x_c, s) \\ \bar{w}_{,x}(x_c, s) \\ 0 \\ 0 \end{Bmatrix}. \tag{12b}$$

Combining equations (12a, b) with the displacement continuity and force balance conditions (5) and (6a, b) leads to the set of equations

$$[T_c(s)]\bar{w}_d(s) = 0, \tag{13}$$

where, for the string,

$$\bar{w}_d(s) = \{\bar{w}(x_c, s)\}, \qquad T_s(s) = \frac{-(1-c^2)}{x_c} H_{22}^{(1,1)} + \frac{(1-c^2)}{1-x_c} H_{21}^{(2,0)} - k_t, \tag{14a,b}$$

and for the beam,

$$\bar{w}_d(s) = \{\bar{w}(x_c, s)\ \bar{w}_{,x}(x_c, s)\}, \tag{15a}$$

$$T_c(s) = \begin{bmatrix} -\dfrac{1}{x_c^2} H_{33}^{(1,1)} + \dfrac{1}{(1-x_c)^2} H_{31}^{(2,0)} & -k_r - \dfrac{1}{x_c^2} H_{34}^{(1,1)} + \dfrac{1}{(1-x_c)^2} H_{32}^{(2,0)} \\ -k_t + \dfrac{1}{x_c^3} H_{43}^{(1,1)} - \dfrac{1}{(1-x_c)^3} H_{41}^{(2,0)} & \dfrac{1}{x_c^3} H_{44}^{(1,1)} - \dfrac{1}{(1-x_c)^3} H_{42}^{(2,0)} \end{bmatrix}, \tag{15b}$$

where $H_{mn}^{(iz)}$ denotes the (m, n) element of $H^{(i)}(z, s)$. The eigenvalues of the system are the roots of the transcendental characteristic equation obtained from

$$\text{Det}\,[T_c(s)] = 0. \tag{16}$$

The eigenfunctions of the constrained axially moving material are obtained by first determining the eigenvalues s_j of the system from equation (16). The corresponding eigenvector $\bar{w}_d(s_j)$ from equation (13) is then back substituted into equation (11) to give the jth eigenfunction

$$w(x, s_j) = h_1^{(i)}(x, s_j)\boldsymbol{\gamma}^{(i)}(s_j), \qquad i = 1, 2, \quad x \in [x_{i-1}, x_i]. \tag{17}$$

4. CRITICAL SPEED

It is well known that both the translating string and beam experience a divergence instability at a critical speed where the fundamental natural frequency becomes zero. For the simply-supported single span, the critical speed for the string is 1 and for the beam it is $\sqrt{p_o + \pi^2}$ [27]. It has been shown that the addition of a point spring to the translating string does not alter its critical speed [4, 5, 20, 28]; i.e., the critical speed remains unchanged regardless of the value of the spring stiffness k_t and the location of the spring x_c.

The effects of the transverse spring on the critical speed of the beam model are shown in Figures 2 and 3 where the first natural frequency is plotted against the translation speed.

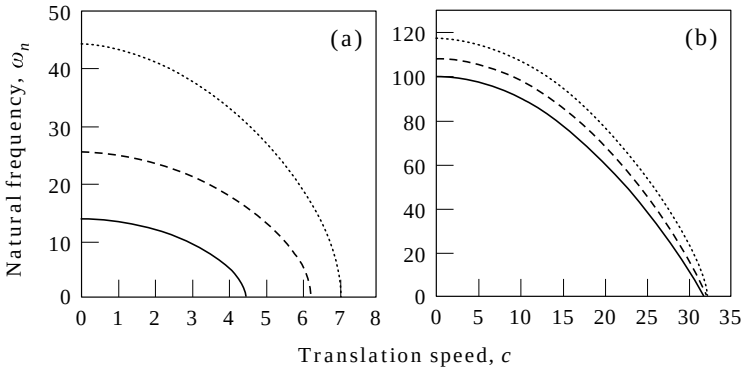

Figure 2. Locus of the first natural frequency of the beam model versus c with $k_t = 2000$, $k_r = 0$; ——, $x_c = 0$; – – –, $x_c = 0{\cdot}25$; · · · · , $x_c = 0{\cdot}5$: (a) $p_o = 10$; (b) $p_o = 1000$.

Figures 2(a, b) illustrate how the critical speed is affected by the location of the point spring. It is seen that the critical speed is smallest when there is no spring ($x_c = 0$ or 1) and largest when the spring is located at the middle of the span ($x_c = 0{\cdot}5$). Due to the symmetry of the problem, all other constraint locations result in a critical speed between these two cases. Note that because the critical speed is the condition for the singularity of the stiffness operator [27], an analogy can be drawn between this problem and the divergence instability of the beam buckling, where the translation speed has the interpretation of the compressive load. For a beam under a spring support, the buckling load increases with spring stiffness and is largest when the spring is located at the middle of the beam [29]. These trends are also observed in Figures 2 and 3.

Comparing Figures 2(a) and (b), it is seen that the critical speed becomes less sensitive to changes in the location of the spring support as the tension becomes large. At sufficiently high tension, the results suggest that the critical speed becomes independent of the location of the spring support. This phenomenon is consistent with the fact that the beam exhibits a "string-like" behaviour under high tension [8, 23]. Figures 3(a, b) show the effects of the spring stiffness on the critical speed. Again, under high tension, the critical speed becomes independent of k_t due to the "string-like" behaviour. However, for low tension, the critical speed increases with k_t and approaches the limit of the critical speed of the moving beam with an intermediate rigid support. Although not shown, simulation results indicate that

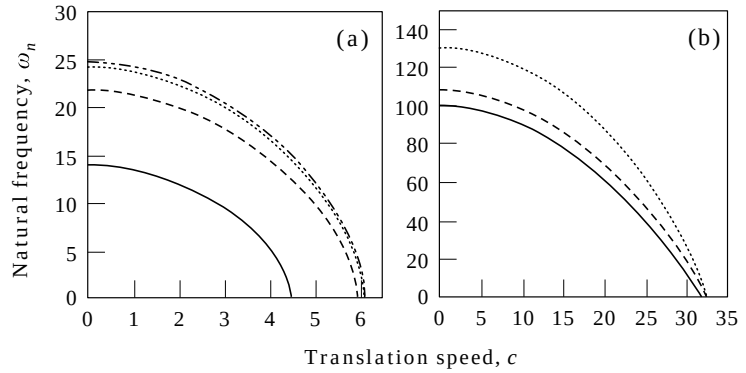

Figure 3. Locus of the first natural frequency of the beam model versus c with $k_r = 0$; ——, $k_t = 0$; – – –, $k_t = 1000$; · · · · , $k_t = 5000$; —·—·—, $k_t = 20\,000$: (a) $p_o = 10$, $x_c = 0{\cdot}2$; (b) $p_o = 1000$, $x_c = 0{\cdot}4$.

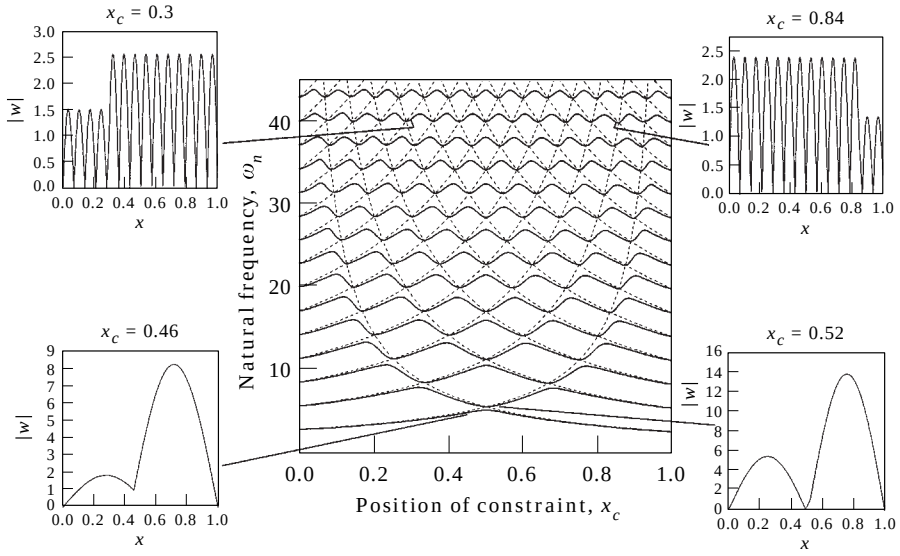

Figure 4. Loci of the natural frequencies of the string model versus x_c for $k_t = 50$, $c = 0{\cdot}3$. Dashed curves (——) are for the case when $k_t \to \infty$. Mode amplitudes for the first, second and 14th modes are also shown.

the addition of a rotational spring gives the same qualitative behaviour as the transverse spring for the critical speed.

5. MODE LOCALIZATION AND WAVE PROPAGATION

5.1. TRANSLATING STRING MODEL

Figure 4 shows the loci of natural frequencies as a function of the position of the constraint x_c with $k_t = 50$. For comparison, natural frequencies of the uncoupled subsystems ($k_t \to \infty$) are also plotted as dashed lines. It has been shown for the stationary string that eigenvalue veering and the degree of mode localization diminish as the natural frequency increases [24]. From Figure 4, it is seen that the translating string also exhibits a similar behaviour. The eigenvalue loci of the lower modes have significant veering and the modes are localized. However, as the natural frequency increases, the amplitudes of the loci curves of the higher modes diminish, becoming increasing flatter relative to the loci of the lower modes and thus mode localization decreases. Simulation results of the mode shapes shown in Figure 4 confirm this behaviour. It is noted that mode localization is discussed in references [21, 22] for a translating string coupled to stationary constraints. However, both discussions were not focused on high frequency behaviour.

To investigate the effects of k_t on the behaviour of the constrained translating string at high frequencies, a wave analysis similar to reference [24] is performed. For this system, the reflection and transmission coefficients are

$$r = \frac{k_t}{-k_t - 2\mathrm{i}\omega}, \qquad t = \frac{2\mathrm{i}\omega}{k_t + 2\mathrm{i}\omega}. \tag{18}$$

It is immediately apparent that both r and t are independent of the translation speed c. That is, the reflection and transmission coefficients for the translating and stationary strings are exactly the same. Thus, for the translating string, it is also true that the degree of mode localization decreases as ω increases regardless of the value of k_t. This is because

as $\omega \to \infty$, $r \to 0$ and $t \to 1$, resulting in all waves being transmitted through the coupling spring.

To gain more insight on the mode localization of the string, the peak amplitude ratio AR is determined. The peak amplitude ratio characterizes the mode localization and is defined as [19]

$$AR = \left|\frac{A_1}{A_2}\right|, \qquad |A_1| \leqslant |A_2|, \tag{19}$$

where A_1 and A_2 are the maximum deflection amplitudes in the spans. The amplitude ratio varies from 0 to 1; the smaller AR is, the more localized the mode. Figure 5 illustrates the effects of c on the peak amplitude ratio of the first mode in the region of loci veering for several values of k_t. In general, the amplitude ratio decreases as c increases. Near the critical speed the mode is highly localized for all values of k_t. It is also seen that as k_t increases, not only does the amplitude ratio decrease, but the curves become increasingly flatter over the entire range of c. This indicates that the effect of the translation speed on the degree of localization diminishes as k_t increases. Thus, at sufficiently high k_t, the mode becomes highly localized over the entire range of c with the amplitude ratio being independent of c.

Figures 6(a, b) show the relationship between the mode shape and the phase in the region of the loci veering for the second mode. Both the real and imaginary parts of the eigenfunction are plotted. As the veering point is crossed, a "mode exchange" is observed for both the real and imaginary parts of the mode shape as well as the phase. A similar behaviour was also observed for a cyclic, two-span axially moving beam [23].

5.2. TRANSLATING BEAM MODEL

For the beam model, the subsystems may be coupled through both transverse and rotational constraints. Previous work has shown that the presence of k_r can significantly alter the behaviour of the stationary, non-tensioned beam [24]. Following the same approach, we will first investigate the effects of only the transverse spring on the beam

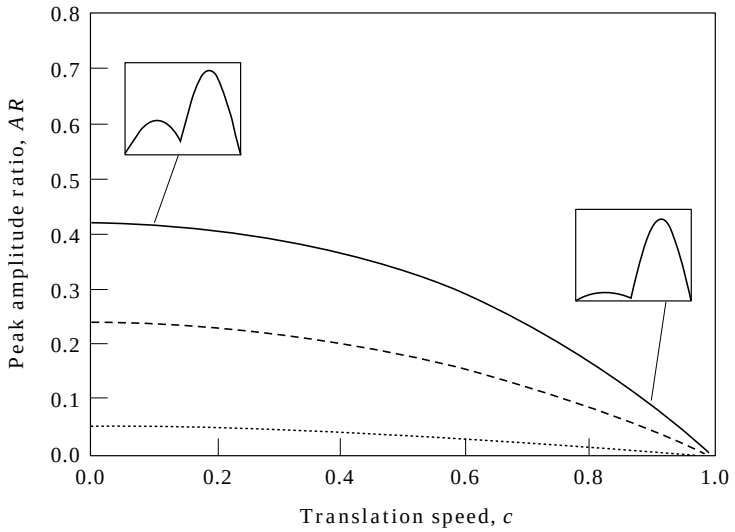

Figure 5. Peak amplitude ratio versus c for the first mode of the string with $x_c = 0{\cdot}48$; ——, $k_t = 50$; – – –, $k_t = 100$; · · · · , $k_t = 500$.

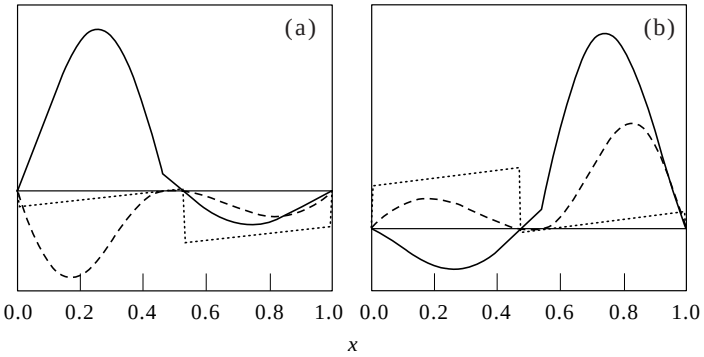

Figure 6. Real (——) and imaginary (– – –) parts of eigenfunctions and phase (· · · ·) for the second mode of the string model with $c = 3$, $k_t = 50$: (a) $x_c = 0{\cdot}46$; (b) $x_c = 0{\cdot}54$.

vibration. Figure 7 shows the natural frequency loci for $k_t = 5000$, $k_r = 0$. The results for $k_t \to \infty$ (dashed curves) are also plotted for reference. Note that for $k_r = 0$, the subsystems are strongly coupled in rotation and weakly coupled in transverse displacement. Thus, the dashed curves are not the eigenvalue loci of the uncoupled subsystems ($k_t, k_r \to \infty$). Nevertheless, comparing with Figure 4, a similar loci veering phenomenon occurs for the first few modes, and veering diminishes as the loci of the higher modes deviate away from the loci of the dashed curves significantly. Again the degree of mode localization diminishes for higher modes. This is clearly shown in Figure 7, where the mode shapes of the seventh mode are plotted for two values of x_c. It is also observed that this decrease in localization is accompanied by an increase in the spacing between successive loci curves. This is consistent with the results of reference [23] in which a "group width", defined as the spacing between pairs of natural frequency loci, was used as an indicator of the strength of the inter-span coupling. The larger the group width, the stronger the inter-span coupling and hence the smaller the degree of localization.

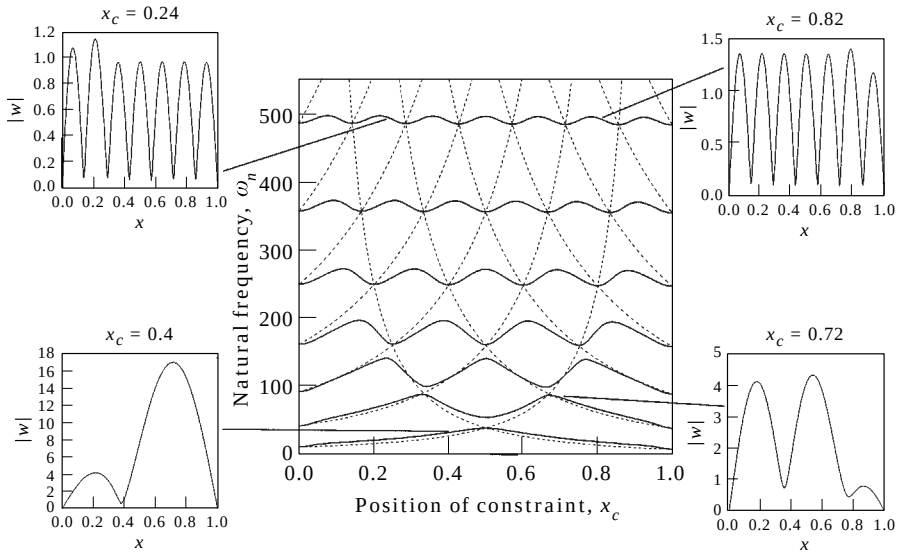

Figure 7. Loci of the natural frequencies of the beam model versus x_c for $k_t = 5000$, $k_r = 0$, $c = 3$ and $p_o = 10$. Dashed curves (– – –) are for the case when $k_t \to \infty$. Representative mode amplitudes are also shown.

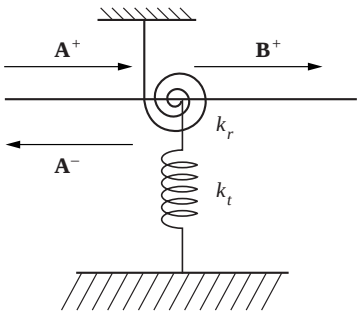

Figure 8. Wave reflection and transmission at the coupling point of the beam system.

To facilitate a better understanding of the effects of system parameters on the beam behaviour, a wave analysis at the subsystem interface is performend. Consider the wave propagation at the interface, as shown in Figure 8. The dispersion relation is

$$-\omega^2 + 2c\gamma_b\omega + (p_o - c^2)\gamma_b^2 + \gamma_b^4 = 0, \tag{20}$$

which results in wavenumbers of the form

$$\gamma_b = a + bi,\ a - bi,\ d,\ -(2a + d) \equiv \gamma_1, \gamma_2, \gamma_3, \gamma_4, \qquad a, b, d > 0. \tag{21}$$

The beam has four wave components: two of which are propagating (γ_3, γ_4) and the other two are propagating and spatially decaying (γ_1, γ_2). At the subsystem interface (denoted by a local variable $\zeta = 0$), the wave solutions are

$$w(\zeta, t) = \begin{cases} A_1\, e^{i(\omega t - \gamma_3\zeta)} + A_2\, e^{i(\omega t - \gamma_2\zeta)} + A_3\, e^{i(\omega t - \gamma_4\zeta)} + A_4\, e^{i(\omega t - \gamma_1\zeta)}, & \zeta < 0^-, \\ B_1\, e^{i(\omega t - \gamma_3\zeta)} + B_2\, e^{i(\omega t - \gamma_2\zeta)}, & \zeta > 0^+. \end{cases} \tag{22}$$

The 2×2 reflection and transmission matrices $\mathbf{r}$ and $\mathbf{t}$ are expressed as [30]

$$\mathbf{A}^- = \mathbf{r}\mathbf{A}^+, \qquad \mathbf{B}^+ = \mathbf{t}\mathbf{A}^+, \tag{23a, b}$$

$$\mathbf{A}^+ = \begin{Bmatrix} A_1 \\ A_2 \end{Bmatrix}, \qquad \mathbf{A}^- = \begin{Bmatrix} A_3 \\ A_4 \end{Bmatrix}, \qquad \mathbf{B}^+ = \begin{Bmatrix} B_1 \\ B_2 \end{Bmatrix}, \qquad \mathbf{r} = \begin{bmatrix} r_{11} & r_{12} \\ r_{21} & r_{22} \end{bmatrix}, \qquad \mathbf{t} = \begin{bmatrix} t_{11} & t_{12} \\ t_{21} & t_{22} \end{bmatrix}, \tag{24}$$

where the superscripts + and − denote the positive and negative propagating directions, r_{i1} and t_{i1}, $i = 1, 2$ are associated with the propagating waves, r_{i2} and t_{i2} are associated with the spatially decaying waves. Applying the continuity of generalized displacements and force balance (6a, b) at the coupling point leads to the set of equations

$$\begin{bmatrix} 1 & 1 \\ -i\gamma_3 & -\gamma_2 \end{bmatrix}\mathbf{A}^+ + \begin{bmatrix} 1 & 1 \\ -i\gamma_4 & -i\gamma_1 \end{bmatrix}\mathbf{A}^- = \begin{bmatrix} 1 & 1 \\ -i\gamma_3 & -i\gamma_2 \end{bmatrix}\mathbf{B}^+, \tag{25}$$

$$\begin{bmatrix} -\gamma_3^2 & -\gamma_2^2 \\ i\gamma_3^3 & i\gamma_2^3 \end{bmatrix}\mathbf{A}^+ + \begin{bmatrix} -\gamma_4^2 & -\gamma_1^2 \\ i\gamma_4^3 & i\gamma_1^3 \end{bmatrix}\mathbf{A}^- = \begin{bmatrix} -\gamma_3^2 & -\gamma_2^2 \\ i\gamma_3^3 & i\gamma_2^3 \end{bmatrix}\mathbf{B}^+ + \begin{bmatrix} i\gamma_3 k_r & i\gamma_2 k_r \\ k_t & k_t \end{bmatrix}\mathbf{B}^+. \tag{26}$$

Resolving equations (25, 26) in the form of equations (23a, b) yields the reflection and transmission matrices $\mathbf{r}$ and $\mathbf{t}$. In this paper, the properties of r_{11} and t_{11} will be examined and compared with those in reference [24] for the stationary, non-tensioned beam.

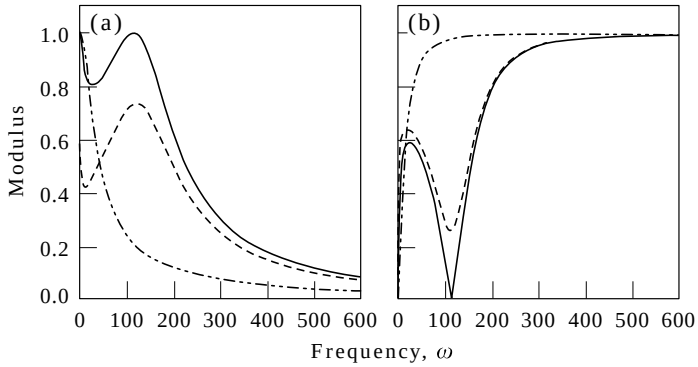

Figure 9. Reflection and transmission coefficients for the beam model with $k_t = 5000$, $k_r = 0$; ——, $c = 0$, $p_o = 10$; – – –, $c = 3$, $p_o = 10$; · · · · , $c = 3$, $p_o = 10\,000$; –··–··–, $c = 60$, $p_o = 10\,000$: (a) r_{11}; (b) t_{11}.

5.2.1. *Strongly coupled in rotation* ($k_r = 0$)

Figures 9(a, b) plot the moduli of the reflection and transmission coefficients as a function of frequency for several different cases. Comparing these curves with those of a stationary beam with no tension (Figure 7 of reference [24]), it is noted that relatively small values of c and p_o have little effects on the behaviour of the reflected and transmitted waves. However, as the tension increases and becomes large ($p_o = 10\,000$), the curves resemble those of the string (Figure 4 of reference [24]). Again this is consistent with the fact that the beam has a "string-like" behaviour as tension becomes large. It is also noted that not only do the curves have the same shape and trend as the string when the tension is large, but both curves for $c = 3$ and $c = 60$ completely overlap each other and are numerically the same. This is consistent with equation (18) which shows that r and t for the string are independent of c. Thus, for large tension, both the translating and stationary beam models exhibit a "string-like" behaviour. The figures also show that, as ω increases, $|t_{11}| \to 1$ and $|r_{11}| \to 0$ independent of the values of c and p_o. Thus, the inter-span coupling of the subsystems becomes strong as ω increases and the degree of mode localization diminishes.

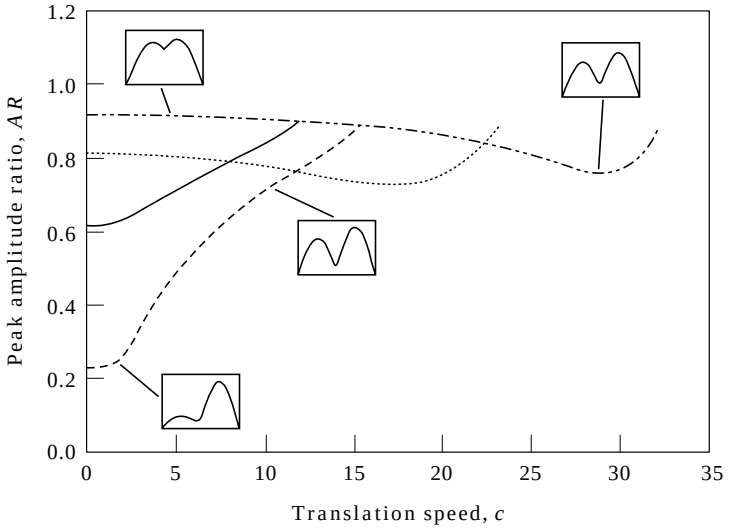

Figure 10. Peak amplitude ratio versus c for the first mode of the beam with $x_c = 0{\cdot}49$, $k_t = 8000$, $k_r = 0$; ——, $p_o = 100$; – – –, $p_o = 200$; · · · · , $p_o = 500$; –··–··–, $p_o = 1000$.

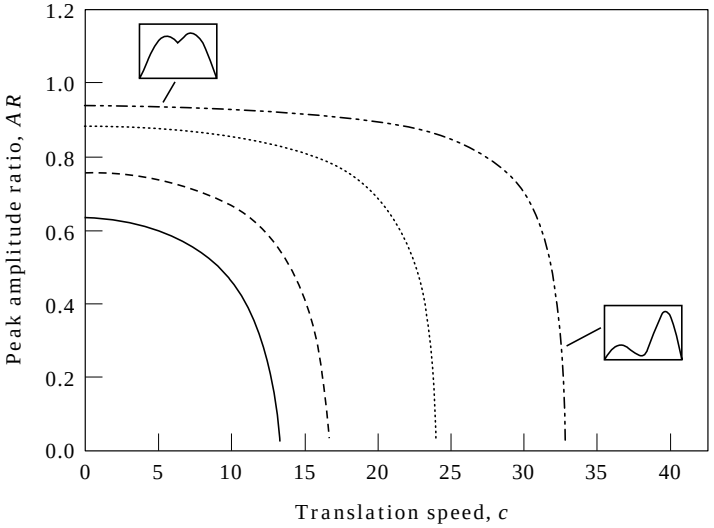

Figure 11. Peak amplitude ratio versus c for the first mode of the beam with $x_c = 0{\cdot}49$, $k_t = k_r = 8000$; ——, $p_o = 100$; – – –, $p_o = 200$; · · · · , $p_o = 500$; –·–·–·–, $p_o = 1000$.

Figure 10 illustrates the effects of speed and tension on the peak amplitude ratio of the first mode in the region of loci veering with $k_r = 0$. For a given tension, the curves are plotted up to the corresponding critical speed. In keeping with the context of mode localization in weakly coupled subsystems, only large values of spring constants are considered. First consider the stationary beam when $c = 0$. Increasing the tension from 100 to 200 decreases the amplitude ratio from 0·61 to 0·23 and hence mode localization increases. However, when the tension is increased to 500, the amplitude ratio jumps up to 0·81, indicating a dramatic decrease in mode localization, and AR continues to increase for higher tension. This suggests that for a given k_t, there is a specific tension p_o^* below which mode localization increases with tension, and above it mode localization decreases with tension. For the translating beam with $p_o < p_o^*$, the amplitude ratio increases with c, with the largest amplitude ratio occurring just below the critical speed. For $p_o > p_o^*$, the curves appear to be relatively flat for low values of c. As the speed is increased, the amplitude ratio starts to decrease until a certain speed is reached where the curves then begin to increase until just below the critical speed. These results clearly indicate that with or without c, for a given k_t there exists a p_o^* which separates the beam behaviour into two different regimes.

From above discussion, it appears that for a translating beam whose sub-spans are strongly coupled in rotation, the effects of c on the amplitude ratio change significantly as the tension is varied. At sufficiently high tension, it can be shown that the curves become flat and the amplitude ratio approaches one, indicating that there is no mode localization and c or k_t have negligible effects on the beam behaviour. In this case the beam behaves as a single span with k_t being transparent to the system. This is because for high tension, the natural frequencies increase and become very large, resulting in waves being completely transmitted through the constraint (see Figure 9).

5.2.2. *Weakly coupled in rotation* (k_r *large*)

In this section, we consider the translating beam which is weakly coupled in both transverse displacement and rotation, and examine the effects of the elastic constraints on the beam vibration. Wave propagation results for this case will be presented in section 6.

Figure 11 shows the relationship between the amplitude ratio and speed for the first mode. The trend of these curves is much different from those of Figure 10, indicating a significant change in the behaviour of the beam due to the presence of the rotational constraint. In general, higher tension leads to larger AR, while an increase of the translation speed reduces AR. In particular, near the critical speed, the amplitude ratio decreases sharply. It is also noted that as tension increases, the curves become increasingly flatter and the amplitude ratio approaches one in the speed range away from the critical speed. This behaviour again demonstrates the diminishing effect of speed on the mode localization as tension increases.

Previous results show that weakly coupled subsystems usually result in weak inter-span coupling [17]. However, our results indicate that weakly coupled subsystems (large k_t and k_r) can experience strong inter-span coupling in their response, especially when the tension in the beam is large. Moreover, comparing Figures 5, 10 and 11, it is noted that for the string and the weakly bi-coupled beam, the mode localization is strongest as the speed approaches the critical speed. Athough not shown, the beam also experiences a mode exchange phenomenon (see Figure 6) as the constraint location is varied in the region of loci veering.

6. MODE DELOCALIZATION

For the stationary, non-tensioned beam with both k_t and k_r, a mode delocalization phenomenon exists whereby a particular mode experiences no localization while neighbouring modes may be localized [24]. This can occur in any mode depending on the parameters of the system. Using the values of k_t and k_r from reference [24], Figure 12 represents the natural frequency loci versus the location of the constraint x_c with $c = 3$, $p_o = 10$. Comparing with Figure 8 of reference [24], it is seen that the fourth mode is also delocalized, even with the additional effects of tension and translation speed. To investigate the effects of the tension and translation speed on the delocalization as well as the high frequency behaviour of the system, the reflection and transmission coefficients at the

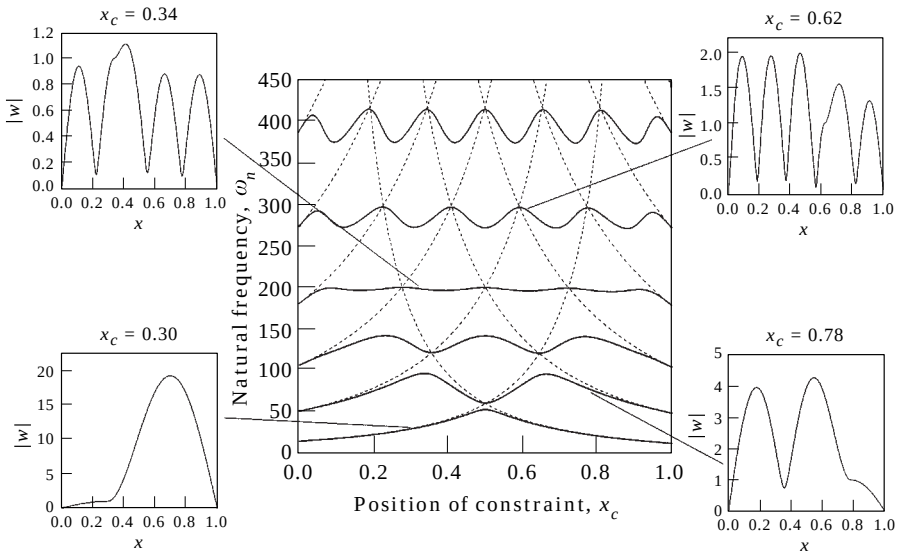

Figure 12. Loci of natural frequencies of the beam model versus x_c with $c = 3$, $p_o = 10$, $k_t = k_r = 5000$. Dashed curves (——) are for the case when $k_t, k_r \to \infty$. Representative mode amplitudes are also shown.

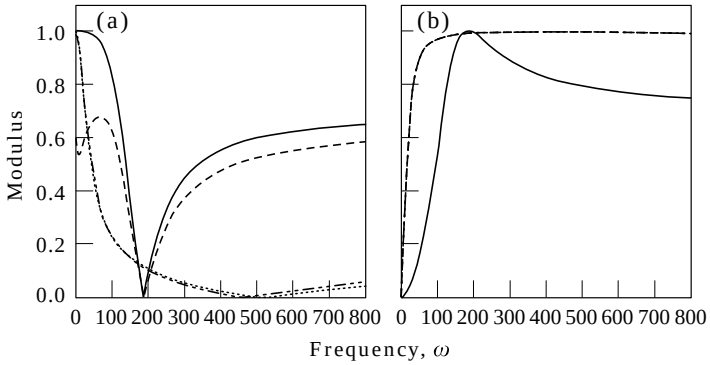

Figure 13. Reflection and transmission coefficients for the beam model with $k_t = k_r = 5000$; ——, $c = 0$, $p_o = 10$; – – –, $c = 3$, $p_o = 10$; · · · · , $c = 3$, $p_o = 10\,000$; –··–··–··–, $c = 60$, $p_o = 10\,000$: (a) r_{11}; (b) t_{11}.

coupling point are determined in a similar manner as before. The moduli of r_{11} and t_{11} are shown in Figure 13 for different values of tension and translation speed. As $\omega \to \infty$, simulation results show that $|r_{11}| \to 0$ and $|t_{11}| \to 1$. Hence, mode localization diminishes as frequency increases and does not occur at sufficiently high frequencies.

Following references [24], the delocalization frequency ω_d is defined as the frequency where $r_{11} = 0$. Figure 13 shows that relatively small values of c and p_o have very little influence on ω_d, while large values of tension can increase ω_d significantly. For large tension, curves for both the reflection and transmission coefficients approach a "string-like" behaviour (compare with Figure 4 of reference [24]). To understand the dependence of ω_d on system parameters, first consider the stationary beam with tension. Equation (20) becomes

$$-\omega^2 + p_o\gamma_b^2 + \gamma_b^4 = 0, \tag{27}$$

which has solutions of the form

$$\beta_1 = \sqrt{\frac{a-b}{2}}, \qquad \beta_2 = -\sqrt{\frac{a-b}{2}}, \qquad \beta_3 = \sqrt{\frac{a+b}{2}}, \qquad \beta_4 = -\sqrt{\frac{a+b}{2}}, \tag{28}$$

where β_1 and β_2 are purely imaginary, β_3 and β_4 are real, and

$$a = -p_o, \qquad b = \sqrt{p_o^2 + 4\omega^2}. \tag{29}$$

Substitute β_i for γ_i, $i = 1, 2, 3, 4$ in equations (25, 26) and solve for $\mathbf{r}$. Setting the numerator of r_{11} equal to zero results in

$$b(\sqrt{a-b} + \sqrt{a+b})(ak_r\sqrt{a-b} + bk_r\sqrt{a-b} - 2k_t\sqrt{a-b} - \mathrm{i}\sqrt{2}k_tk_r) = 0. \tag{30}$$

Since b and the first parenthesis can never be zero for real and positive frequency, rewriting the terms in the second parenthesis gives

$$a + b - \frac{2k_t}{k_r} - \frac{\mathrm{i}\sqrt{2}k_t}{\sqrt{a-b}} = 0 \tag{31}$$

or

$$-p_o + \sqrt{p_o^2 + 4\omega_d^2} - \frac{2k_t}{k_r} - \frac{\mathrm{i}\sqrt{2}k_t}{\sqrt{-p_o - \sqrt{p_o^2 + 4\omega_d^2}}} = 0. \tag{32}$$

Solving equation (32) numerically gives two roots for ω. These roots have the form of $\pm\alpha$. The positive root gives ω_d. As $p_o \to 0$, equation (32) recovers the equation for the beam without tension [24], that is

$$\omega_d^{3/2} - \omega_d^{1/2}\left(\frac{k_t}{k_r}\right) - \frac{k_t}{2} = 0. \tag{33}$$

It can be shown that, for small values of p_o, equation (33) gives a reasonable approximation of ω_d. Moreover, it is seen that as $p_o \to \infty$ and for finite ω_d, equation (32) yields

$$k_t/k_r = 0, \tag{34}$$

which has no solution for ω_d and hence delocalization cannot occur. Since delocalization does not occur for the string model, this result again demonstrates that the beam has a "string-like" behaviour under sufficiently large tension.

In general, both k_t and k_r are needed for the mode delocalization to occur and the value of ω_d depends on these parameters. However, equation (33) shows that when $k_r \to \infty$ (mono-coupled in transverse displacement), mode delocalization can occur. While for $k_t \to \infty$, it cannot occur. This is also true for the non-tensioned beam. Equations (32) and (33) also indicate that, unlike mode localization where coupling is usually weak (large k_t and k_r), ω_d can exist for any value of k_t and k_r, whether large or small. Figure 14 illustrates the relationships between the delocalization frequency and p_o and k_t with $k_r = 50$. In general, ω_d increases with p_o and k_t. Results for different values of k_r (not shown) show a similar trend for ω_d versus p_o and k_t. However, an increase in k_r results in a decrease in the value of ω_d.

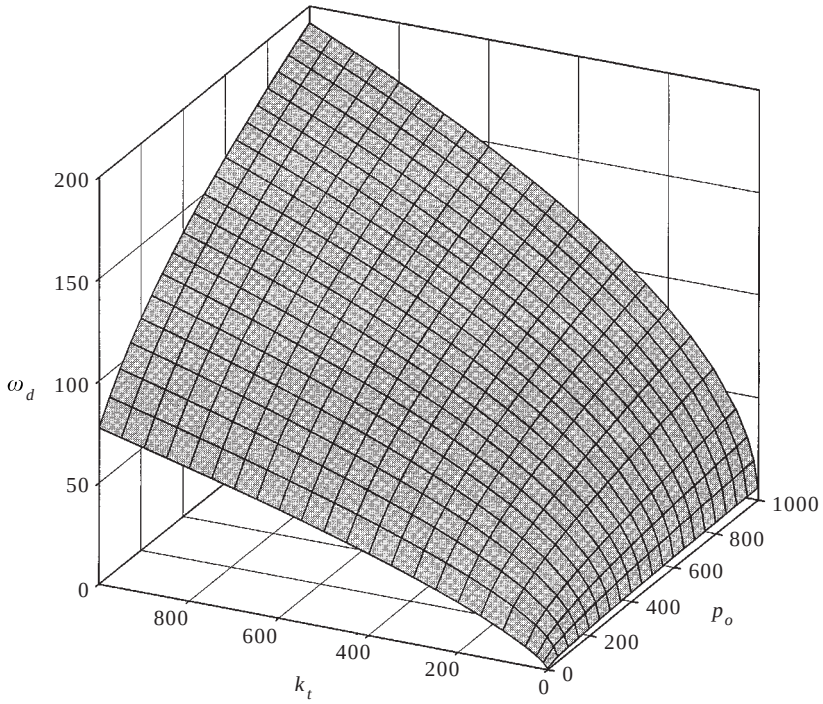

Figure 14. Delocalization frequency versus p_o and k_t with $c = 0$, $k_r = 50$.

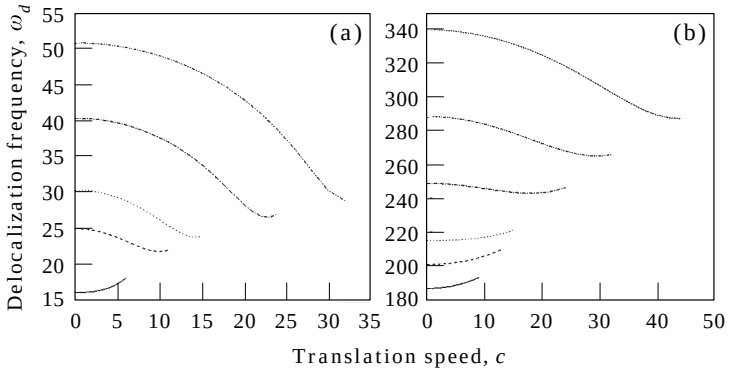

Figure 15. Delocalization frequency versus c; ——, $p_o = 10$; — —, $p_o = 100$; · · · ·, $p_o = 200$; —·—·—, $p_o = 500$; —··—··—, $p_o = 1000$; ---, $p_o = 2000$: (a) $k_t = k_r = 100$; (b) $k_t = k_r = 5000$.

Due to the size and complexity of r_{11}, closed-form analytical results of ω_d for the translating case are not presented. However, simulation results of $|r_{11}|$ for other support conditions analyzed in reference [24] confirm that the delocalization for the translating beam occurs in the same two cases as that of the stationary, non-tensioned beam, namely, when both k_t and k_r are non-zero and finite or when $k_r \to \infty$ and k_t is non-zero and finite. When $c \neq 0$, the equation which determines the delocalization frequency has the same form as equation (32):

$$\lambda_1 + \lambda_2\left(\frac{k_t}{k_r}\right) + \lambda_3 k_t = 0, \tag{35}$$

where $\lambda_{1,2,3}$ are a function of tension, speed and frequency. The results presented here are for $k_t = k_r$. Figure 15(a) and (b) plot ω_d versus c (up to critical speed) for relatively small and large values of spring stiffness, respectively. In Figure 15(a), for $p_o = 10$, ω_d increases with the translation speed. For $p_o \geqslant 100$, the general trend of the curves show a decrease in ω_d as c increases. In Figure 15(b), the trend is that ω_d increases (or decreases) for tension roughly smaller (or larger) than 500. Thus, it appears that for a given k_t and k_r, there is a specific tension which separates two regions of different behaviour. Below this tension, ω_d increases with speed while above it ω_d tends to decrease as c increases. It is believed that below this tension, the effects of c and k_t dominate the behaviour of the beam and cause ω_d to increase. However, above this tension, the effect of tension dominates, resulting in the decrease of ω_d with the speed. It can also be seen from the figures that as the critical speed is approached, the curves for the higher values of p_o tend to flatten out (indicating that effects of c and p_o "cancel out") and in some cases they start to increase, which is most likely due to the contribution from the effects of speed.

7. SUMMARY AND CONCLUSIONS

In this paper, the free response of an elastically constrained, axially moving string and beam is examined. In particular, the effects of system parameters on the critical speed, mode localization and delocalization of the system are presented. Conclusions are summarized as follows.

For low tension, the addition of a transverse and/or rotational spring to the beam model increases its critical speed. In general, the value of the critical speed depends on the value

of the spring constants, the location of the constraint and tension. For sufficiently large tension, the critical speed of the beam becomes independent of the spring constraints.

For the string model, mode localization increases with the translation speed and is strongest as the critical speed is approached. However, when the spring stiffness is large, the degree of mode localization is predominantly determined by the stiffness rather than the speed.

For both the string and beam models, a wave analysis shows that eigenvalue veering and mode localization diminish as the natural frequency increases. This result is independent of the system parameters. Thus, the lower modes are always more strongly localized than the higher modes.

The effects of speed and tension on mode localization of the bi-coupled beam depend strongly on the type of coupling. For the beam with just k_t, no general trends regarding the effects of speed and tension on mode localization exist. For the beam with both k_t and k_r, localization increases with speed and decreases with tension. Results also show that weakly coupled subsystems can experience strong inter-span coupling in their response, especially when the tension in the beam is large.

Mode delocalization still occurs for the axially moving bi-coupled beam. The delocalization frequency ω_d increases with the tension, while increasing speed can increase or decrease ω_d depending on the tension and spring constants. The mode delocalization represents another example of weakly coupled subsystems exhibiting strong inter-span coupling.

In terms of wave propagation, critical speed, and delocalization, the beam with k_t and the beam with k_t and k_r both exhibit a "string-like" behaviour when tension is sufficiently large. However, for mode localization, only the beam with both k_t and k_r behaves similar to the string model.

ACKNOWLEDGMENT

The authors gratefully acknowledge the support of the National Science Foundation, Ford Motor Company and the Institute for Manufacturing Research of Wayne State University for this research work.

REFERENCES

1. A. Simpson 1973 *Journal of Mechanical Engineering Science* **15**, 159–164. Transverse modes and frequencies of beams translating between fixed end supports.
2. C. D. Mote, Jr. 1965 *Journal of the Franklin Institute* **279**, 430–444. A study of bandsaw vibrations.
3. J. A. Wickert and C. D. Mote, Jr. 1988 *Shock and Vibration Digest* **50**, 3–13. Current research on the vibration and stability of axially moving materials.
4. G. S. Schajer 1984 *Journal of Sound and Vibration* **92**, 11–19. The vibration of a rotating circular string subject to a fixed elastic constraint.
5. N. C. Perkins 1990 *ASME Journal of Vibration and Acoustics* **112**, 2–7. Linear dynamics of a translating string on an elastic foundation.
6. A. G. Ulsoy, J. E. Whitesell and M. D. Hooven 1985 *ASME Journal of Vibration, Acoustics, Stress, and Reliability in Design* **107**, 282–290. Design of belt–tensioner systems for dynamic stability.
7. A. G. Ulsoy and C. D. Mote, Jr. 1982 *ASME Journal of Engineering for Industry* **104**, 71–78. Vibration of wide band saw blades.
8. C. D. Mote, Jr. and W. Z. Wu 1985 *Journal of Sound and Vibration* **102**, 1–9. Vibration coupling in continuous belt and band systems.
9. K. W. Wang 1991 *ASME Journal of Vibration and Acoustics* **113**, 62–68. Dynamic stability analysis of high speed axially moving bands with end curvatures.

10. K. W. Wang and C. D. Mote, Jr. 1986 *Journal of Sound and Vibration* **109**, 237–258. Vibration coupling analysis of band/wheel mechanical systems.
11. A. G. Ulsoy 1986 *ASME Journal of Vibration, Acoustics, Stress, and Reliability in Design* **108**, 207–212. Coupling between spans in the vibration of axially moving materials.
12. O. O. Bendiksen 1987 *AIAA Journal* **25**, 1241–1248. Mode localization phenomena in large space structures.
13. P. T. Chen and J. H. Ginsberg 1992 *ASME Journal of Vibration and Acoustics* **114**, 141–148. On the relationship between veering of eigenvalue loci and parameter sensitivity of eigenfunctions.
14. C. H. Hodges 1982 *Journal of Sound and Vibration* **82**, 411–424. Confinement of vibration by structural irregularity.
15. C. H. Hodges and J. Woodhouse 1983 *Journal of the Acoustical Society of America* **74**, 894–905. Vibration isolation from irregularity in a nearly periodic structure: theory and measurements.
16. S. D. Lust, P. P. Friedmann and O. O. Bendiksen 1993 *AIAA Journal* **31**, 348–355. Mode localization in multispan beams.
17. C. Pierre 1988 *Journal of Sound and Vibration* **126**, 485–502. Mode localization and eigenvalue loci veering phenomena in disordered structures.
18. C. Pierre and E. H. Dowell 1987 *Journal of Sound and Vibration* **114**, 549–564. Localization of vibrations by structure irregularity.
19. C. Pierre, D. M. Tang and E. H. Dowell 1987 *AIAA Journal* **25**, 1249–1257. Localized vibrations of disordered multispan beams: theory and experiment.
20. S. P. Cheng and N. C. Perkins 1991 *Journal of Sound and Vibration* **144**, 281–292. The vibration and stability of a friction guided, translating string.
21. C. A. Tan and L. Zhang 1994 *Journal of Vibration and Acoustics* **116**, 318–325. Dynamic characteristics of a constrained string translating across an elastic foundation.
22. S. Y. Lee and C. D. Mote 1997 *Proceedings of Fifth Pan American Congress of Applied Mechanics—PACAM V, San Juan, Puerto Rico* **4**, 478–481. Mode localization in a translating medium coupled to stationary constraints.
23. A. A. N. Al-Jawi, C. Pierre and A. G. Ulsoy 1995 *Journal of Sound and Vibration* **179**, 243–266. Vibration localization in dual-span, axially moving beams, Part I: formulation and results.
24. C. H. Riedel and C. A. Tan 1997 *Proceedings of the ASME Design Engineering Technical Conference, Sacramento, CA, Paper DETC97/VIB-3951*. Mode localization and delocalization in constrained string and beams; also submitted to *ASME Journal of Vibration and Acoustics*.
25. B. Yang and C. A. Tan 1992 *ASME Journal of Applied Mechanics* **59**, 1009–1014. Transfer functions of one-dimensional distributed parameter systems.
26. C. A. Tan and C. H. Chung 1993 *ASME Journal of Applied Mechanics* **60**, 1004–1011. Transfer function formulation of constrained distributed parameter systems, Part I: theory.
27. J. A. Wickert and C. D. Mote, Jr. 1990 *ASME Journal of Applied Mechanics* **57**, 738–744. Classical vibration analysis of axially moving continua.
28. J. S. Chen 1997 *ASME Journal of Vibration and Acoustics* **119**, 152–157. Natural frequencies and stability of an axially-traveling string in contact with a stationary load system.
29. S. P. Timoshenko and J. M. Gere 1961 *Theory of Elastic Stability*, Art. 2.6. New York: McGraw-Hill.
30. B. R. Mace 1984 *Journal of Sound and Vibration* **97**, 237–246. Wave reflection and transmission in beams.

APPENDIX: STATE MATRICES AND BOUNDARY OPERATORS

The state matrices and the boundary operators in local co-ordinates for the string are

$$F^{(1)}(s) = \begin{bmatrix} 0 & 1 \\ \dfrac{s^2 x_c^2}{1-c^2} & \dfrac{2csx_c}{1-c^2} \end{bmatrix}, \qquad F^{(2)}(s) = \begin{bmatrix} 0 & 1 \\ \dfrac{s^2(1-x_c)^2}{1-c^2} & \dfrac{2cs(1-x_c)}{1-c^2} \end{bmatrix},$$

$$M^{(i)}(s) = \begin{bmatrix} 1 & 0 \\ 0 & 0 \end{bmatrix}, \qquad N^{(i)}(s) = \begin{bmatrix} 0 & 0 \\ 1 & 0 \end{bmatrix}, \qquad i = 1, 2.$$

The state matrices and the boundary operators in local co-ordinates for the beam are

$$F^{(1)}(s) = \begin{bmatrix} 0 & 1 & 0 & 0 \\ 0 & 0 & 1 & 0 \\ 0 & 0 & 0 & 1 \\ -s^2 x_c^4 & -2csx_c^3 & (p_o - c^2)x_c^2 & 0 \end{bmatrix},$$

$$F^{(2)}(s) = \begin{bmatrix} 0 & 1 & 0 & 0 \\ 0 & 0 & 1 & 0 \\ 0 & 0 & 0 & 1 \\ -s^2(1-x_c)^4 & -2cs(1-x_c)^3 & (p_o - c^2)(1-x_c)^2 & 0 \end{bmatrix},$$

$$M^{(1)}(s) = \begin{bmatrix} 1 & 0 & 0 & 0 \\ 0 & 0 & \frac{1}{x_c^2} & 0 \\ 0 & 0 & 0 & 0 \\ 0 & 0 & 0 & 0 \end{bmatrix}, \qquad N^{(1)}(s) = \begin{bmatrix} 0 & 0 & 0 & 0 \\ 0 & 0 & 0 & 0 \\ 1 & 0 & 0 & 0 \\ 0 & \frac{1}{x_c} & 0 & 0 \end{bmatrix},$$

$$M^{(2)}(s) = \begin{bmatrix} 1 & 0 & 0 & 0 \\ 0 & \frac{1}{1-x_c} & 0 & 0 \\ 0 & 0 & 0 & 0 \\ 0 & 0 & 0 & 0 \end{bmatrix}, \qquad N^{(2)}(s) = \begin{bmatrix} 0 & 0 & 0 & 0 \\ 0 & 0 & 0 & 0 \\ 1 & 0 & 0 & 0 \\ 0 & 0 & \frac{1}{(1-x_c)^2} & 0 \end{bmatrix}.$$